Prediction of the dynamic oscillation threshold in a clarinet model with a linearly increasing blowing pressure

Baptiste Bergeot, André Almeida, Christophe Vergez, Bruno Gazengel

▶ **To cite this version:**

Baptiste Bergeot, André Almeida, Christophe Vergez, Bruno Gazengel. Prediction of the dynamic oscillation threshold in a clarinet model with a linearly increasing blowing pressure. 2012. hal-00719228v1

HAL Id: hal-00719228

https://hal.science/hal-00719228v1

Preprint submitted on 19 Jul 2012 (v1), last revised 27 Nov 2014 (v4)

HAL is a multi-disciplinary open access archive for the deposit and dissemination of scientific research documents, whether they are published or not. The documents may come from teaching and research institutions in France or abroad, or from public or private research centers.

L'archive ouverte pluridisciplinaire **HAL**, est destinée au dépôt et à la diffusion de documents scientifiques de niveau recherche, publiés ou non, émanant des établissements d'enseignement et de recherche français ou étrangers, des laboratoires publics ou privés.

Prediction of the dynamic oscillation threshold in a clarinet model with a linearly increasing blowing pressure

B. Bergeot[a,*], A. Almeida[a], C. Vergez[b], B. Gazengel[a]

[a] *Laboratoire d'Acoustique de l'Université du Maine (LAUM-CNRS UMR 6613), Avenue Olivier Messiaen, 72085 Le Mans Cedex 9, France*

[b] *Laboratoire de Mécanique et Acoustique (LMA-CNRS UPR 7051), 31 Chemin Joseph Aiguier, 13402 Marseille Cedex 20, France*

Abstract

Reed instruments are modeled as self-sustained oscillators driven by the pressure inside the mouth of the musician. A set of nonlinear equations connects the control parameters (mouth pressure, lip force) to the system output, hereby considered as the mouthpiece pressure. Clarinets can then be studied as dynamical systems, their steady behavior being dictated uniquely by the values of the control parameters. Considering the resonator as a lossless straight cylinder is a dramatic yet common simplification that allows for simulations using nonlinear iterative maps.

In this paper, we investigate analytically the effect of a time-varying blowing pressure on the behavior of this simplified clarinet model. When the control parameter varies, results from the so-called *dynamic* bifurcation theory are required to properly analyze the system. This study highlights the phenomenon of *bifurcation delay* and defines a new quantity, the *dynamic oscillation threshold*. A theoretical estimation of the *dynamic oscillation threshold* is proposed and compared with numerical simulations.

Keywords: Musical acoustics, Clarinet-like instruments, Iterated maps, Dynamic Bifurcation, Bifurcation delay, Transient processes.

1 Introduction

One of the interests of mathematical models of musical instruments is to be able to predict certain characteristics of the produced sound given the gesture performed by the musician. In the case of a clarinet for instance, the amplitude, frequency or spectral content (the sound parameters) can be to

*Corresponding author, baptiste.bergeot@univ-lemans.fr

a certain extent, determined as a function of the blowing pressure and lip force applied to the reed (the control parameters). A basic model, such as the one introduced by Mcintyre et al. [1], allows to compute the amplitude of the oscillating resonator pressure from the knowledge of these two control parameters, giving results that follow the major tendencies observed in experiments. Several degrees of refinement can be added to this model, usually aiming at realistic sound and mechanical behavior. Well known simplifications of this model allow to study analytically the behavior of the clarinet. Simplified models, of course, are unable to describe or predict with refinement the exact harmonic content of the sound, or the influences of such important details as the reed geometry and composition or the vocal tract of the player. However, they can provide an understanding of the factors essential for the production of sound.

The highest degree of simplification of the model (introduced in Section 2) considers a straight, lossless (or losses independent of frequency) resonator and the reed as an ideal spring [2, 3, 4]. With these assumptions, the system can be simply described by an iterated map [1]. Iterated maps often describe a succession of different regimes with variable periodicity. By analyzing the asymptotic values of these regimes it is possible to estimate: thresholds of oscillation, extinction, beating regimes, etc. [5], amplitudes and stability of the steady state regime [6] and phenomena of period doubling [7, 8].

These characteristics arise from the so-called *static* bifurcation theory assuming that control parameters are constant. For example, these studies allow to find a *static* oscillation threshold γ_{st} [5] such that a constant regime is stable if the blowing pressure is below γ_{st} and a periodic regime is stable if it is above γ_{st}. This behavior is static, obtained by choosing a constant blowing pressure, letting the system reach its final state, and repeating the procedure for other constant blowing pressures. Therefore, most studies using iterated map approach are restricted to a steady state analysis of the oscillation. They focus on the asymptotic amplitude regardless of the history of the system.

During a note attack transient the musician varies the pressure in her/his mouth before reaching a quasi-constant value. During this transient the blowing pressure cannot be regarded as constant. In a mathematical point of view increasing the control parameter (here the blowing pressure) makes the system non-autonomous and results from *static* bifurcation theory are not sufficient to describe its evolution. Indeed, it is known that, when the control parameter varies, the bifurcation point – i.e. the value of the blowing pressure where the system begins to oscillate – can be considerably delayed [9, 10, 11]. Indeed, the bifurcation point is shifted from γ_{st} to a larger value γ_{dt} called *dynamic* oscillation threshold. This phenomenon called *bifurcation delay* is not predicted by the *static* theory. Therefore, when the control parameter varies, results from the so-called *dynamic* bifurcation theory are required to properly analyze the system.

The purpose of this paper is to use results from *dynamic* bifurcation theory to describe analytically a simplified clarinet model taking into account a blowing pressure that varies linearly with time. In

particular we propose a theoretical estimation of the dynamic oscillation threshold.

Section 2 introduces the simplified mathematical model of a clarinet and the iterated map method used to estimate the existence of the oscillations inside the bore of the clarinet. Some results related to the steady state are presented in this section. Section 3 is devoted to the study of the dynamic system that takes into account a time-varying blowing pressure. The phenomenon of bifurcation delay is demonstrated using numerical simulations. A theoretical estimation of the *dynamic oscillation threshold* is also presented and compared with numerical simulations. In Section 4 the limits of this approach are discussed. It is shown, when the model is simulated, that the precision (the number of decimal digits used by the computer) has a dramatic influence on the bifurcation delay. The influence of the speed at which the blowing pressure is swept is also discussed.

2 State of the art

2.1 Elementary model

The model of the clarinet system used in this article follows an extreme simplification of the instrument, which can be found in other theoretical works [2, 4]. Although it is not suitable to describe the detailed content of the sound produced by the instrument, it is an useful tool to predict the magnitude of certain key features of the instrument, such as the threshold of oscillation, or to estimate the amplitudes of the pressure oscillation inside the instrument.

This basic model separates the instrument into two functional elements. One of these is the bore, or resonator, a linear element where the pressure waves propagate without losses. The other is the reed-mouthpiece system, which is considered as a valve controlled by the pressure difference between the mouth and the mouthpiece. It is often called the generator and is the only nonlinear part of the instrument.

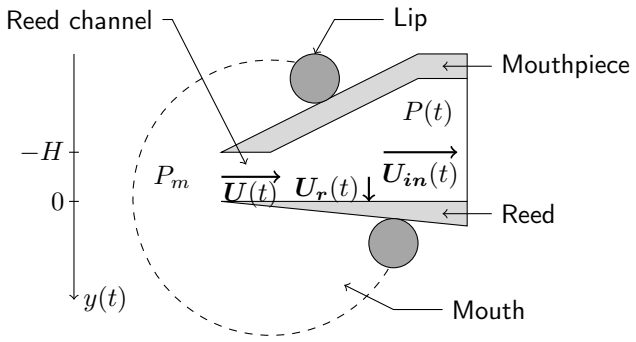

Figure 1: Schematic diagram of a single-reed mouthpiece. Presentation of variables, control parameters and choice of axis orientation. U is the flow created by the pressure imbalance $P_m - P$ between the mouth and the bore, U_r is the flow created by the motion of the reed, U_{in} is the flow entering the instrument, y represents the position of the tip of the reed and H is the opening of the reed channel at rest.

2.1.1 The reed-mouthpiece system

The reed-mouthpiece system is depicted in Fig. 1. The reed is assumed to behave as an ideal spring characterized by its static stiffness per unit area K_s. So, its response y to the pressure difference $\Delta P = P_m - P$ is linear and is given by:

$$y = -\frac{\Delta P}{K_s}. \tag{1}$$

From (1) we can define the *static closing pressure* P_M which corresponds to the lowest pressure that completely closes the reed channel ($y = -H$):

$$P_M = K_s H. \tag{2}$$

The reed model also considers that the flow created by the motion of the reed U_r is equal to zero, so that the only flow entering the instrument is created by the pressure imbalance between the mouth and the bore:

$$U_{in} = U. \tag{3}$$

The non-linearity of the reed-mouthpiece system is introduced by the Bernoulli equation which relates the flow U to the acoustic pressure P [12, 13]. This relation is the nonlinear characteristics of the exciter, given by:

$$U = \begin{cases} U_A \left(1 - \dfrac{\Delta P}{P_M}\right) \sqrt{\dfrac{|\Delta P|}{P_M}} \operatorname{sgn}(\Delta P) \text{ if } \Delta P < P_M & \text{(4a)} \\ 0 \text{ if } \Delta P > P_M. & \text{(4b)} \end{cases}$$

The flow U_A is calculated using the Bernoulli theorem:

$$U_A = S\sqrt{\frac{2P_M}{\rho}}, \tag{5}$$

where S is the opening cross section of the reed channel at rest and ρ the density of the air.

Introducing the dimensionless variables and control parameters [4]:

$$\Delta p = \frac{\Delta P}{P_M} \quad ; \quad p = \frac{P}{P_M} \quad ; \quad u = Z_c \frac{U}{P_M} \quad ; \quad \gamma = \frac{P_m}{P_M} \quad ; \quad \zeta = Z_c \frac{U_A}{P_M}, \tag{6}$$

equation (4) becomes:

$$u = F(p) = \begin{cases} \zeta\,(1-\gamma+p)\,\sqrt{|\gamma-p|}\,\mathrm{sgn}(\gamma-p) \text{ if } \gamma-p<1 & \text{(7a)} \\ 0 \text{ if } \gamma-p>1. & \text{(7b)} \end{cases}$$

The parameters γ and ζ are the control parameters of the system. An example of the function F is shown in Fig. 2(a).

2.1.2 The resonator

Assuming that only plane waves exist in the resonator and propagate linearly, the resonator can be characterized by its reflection function $r(t)$. The general expression relating $p(t)$ to $u(t)$ through $r(t)$ is:

$$p(t) - u(t) = [r * (p+u)](t). \tag{8}$$

The resonator is modeled as a straight cylinder. Reflections at the open end of the resonator are considered perfect (no radiation losses) and viscous and thermal losses are neglected. In this case the reflection function becomes a simple delay with sign inversion:

$$r(t) = -\delta(t-\tau), \tag{9}$$

where δ is the Dirac generalized function and $\tau = 2l/c$ is the round trip travel time of the sound wave with velocity c along the resonator of length l.

With the reflection function (9), equation (8) becomes:

$$p(t) - u(t) = -\left[p(t-\tau) + u(t-\tau)\right]. \tag{10}$$

Using a discrete time formulation (the discretization is done at regular intervals τ) and noting $p(n\tau) = p_n$ and $u(n\tau) = u_n$, we obtain the following difference equation:

$$p_n - u_n = -\left(p_{n-1} + u_{n-1}\right). \tag{11}$$

2.2 Iterated map: outgoing and incoming wave representation

In linear acoustics any planar wave can be expanded into an outgoing wave p^+ and an incoming wave p^-. Using the dimensionless variables defined in equation (6), the acoustic pressure p and flow u are given by:

$$p = p^+ + p^- \qquad ; \qquad u = p^+ - p^-, \tag{12}$$

Replacing in equation (11),

$$p^+ = \frac{1}{2}(p+u) \qquad ; \qquad p^- = \frac{1}{2}(p-u). \tag{13}$$

By combining equations (7) and (12) a nonlinear relation G between p^+ and p^- can be obtained:

$$p^+ = G\left(-p^-\right). \tag{14}$$

An explicit expression of the function G was determined, for $\zeta < 1$, by Taillard et al. [8]. Fig. 2(b) shows an example of the function G. Using equations (12), the relation (11) becomes:

$$p_n^- = -p_{n-1}^+. \tag{15}$$

Finally, equations (14) and (15) define the iterated map:

$$p_n^+ = G\left(-p_n^-\right) = G\left(p_{n-1}^+\right). \tag{16}$$

In the following, the variable p^+ will be used preferentially. The variable p can easily be calculated using equations (15) and (12).

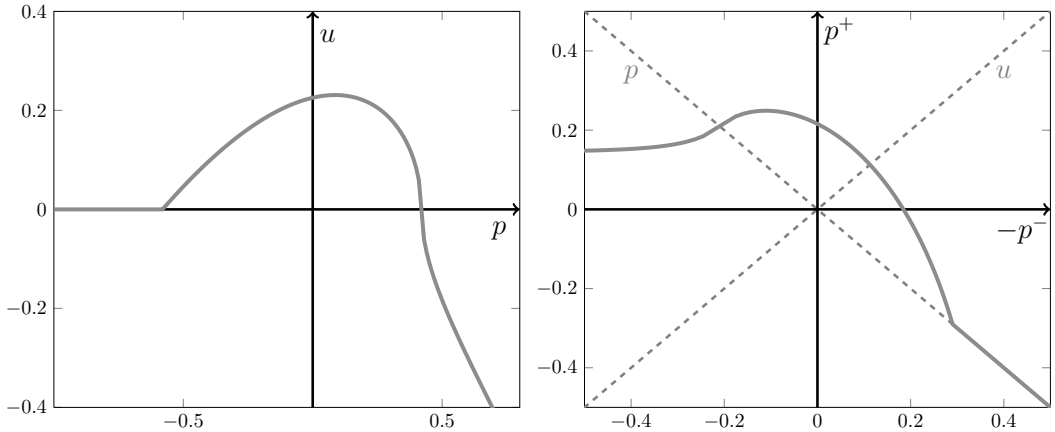

(a) function F (b) function G

Figure 2: Nonlinear characteristics in $u = F(p)$ representation (a) and $p^+ = G(-p^-)$ representation (b) for $\gamma = 0.42$ and $\zeta = 0.6$.

2.3 Results from static bifurcation theory

The difference equation (16) can be analyzed using the *static* bifurcation theory, which assumes that the control parameters are constant. This will be hereafter referred to as the *static case*. The parameter γ will be specifically introduced as a subscript in the definition of the nonlinear characteristics (16), stressing that this will be the parameter of interest in the current study (ζ will always consider to be constant):

$$p_n^+ = G_\gamma\left(p_{n-1}^+\right). \tag{17}$$

Some of the predictions of the *static* bifurcation theory that are important to this work are recalled in the following sections while applying them to the map of equation (17) [14, 4, 8].

2.3.1 Expression of the static regime and static oscillation threshold

For all values of the control parameter γ below a particular value of the parameter γ called *static oscillation threshold* and noted γ_{st} the series p_n^+ converges to a single value (the static regime), also referred to as the fixed point of G_γ. It can be found by solving the following equation:

$$p^{+*} = G_\gamma\left(p^{+*}\right). \tag{18}$$

After solving the equation we obtain :

$$p^{+*}(\gamma) = \frac{\zeta}{2}(1-\gamma)\sqrt{\gamma}. \tag{19}$$

When the static regime is reached $p_n^+ = p_{n-1}^+ = -p_n^-$. Therefore, for the the variable $p = p^+ + p^-$, the static regime is equal to zero.

The static regime exists for all values of the parameter γ but it is stable when $\gamma < \gamma_{st}$ and unstable when $\gamma > \gamma_{st}$. The condition of stability of the static regime [14] allowing to obtain the value of the static oscillation threshold is:

$$\left|G'_\gamma\left(p^{+*}\right)\right| < 1, \tag{20}$$

where G'_γ is the first derivative of the function G. The value of the static oscillation threshold is finally:

$$\gamma_{st} = \frac{1}{3}. \tag{21}$$

Beyond the oscillation threshold, other bifurcations occur, the 2-valued oscillating regime becoming unstable and giving rise to a 4-valued oscillating state. This cascade is the classical scenario of successive period doublings, leading eventually to chaos [15, 8]. The values of the parameter γ for which appear

the different 2n-valued oscillating regimes depend on the value of the parameter ζ: the smaller is ζ, the earlier the 2n-valued oscillating regimes appear. When $\gamma = 1/2$, whatever the value of ζ, a 2-valued oscillating regime reappears, the beating-reed regime . This is a particularity of model of the clarinet, it is due to the fact that when $\gamma - p > 1$ (equation (7b)) the reed presses against the mouthpiece lay. It can be shown [4] that in this permanent regime $p = \pm\gamma$ (c.f. Fig. 3).

2.3.2 *Static* bifurcation diagrams

Common representations of the *static* bifurcation diagram for clarinets usually show the steady state of the pressure inside the mouthpiece p or that of its amplitude (corresponding in the lossless model to the absolute value of p) with respect to the control parameter γ [5]. In this paper, calculations are based on p^+, so that most bifurcation diagrams will represent the steady state of the outgoing wave [8].

Fig. 3 shows an example of these three representations of the *static* bifurcation diagram for $\zeta = 0.5$. Fig. 3 represents only the two first branches of the diagrams. The first branch corresponds to the fixed points of the function G_γ and the second branch represents the fixed points of the function $(G_\gamma \circ G_\gamma)$. On the right figure, the dashed line represents the curve of the static regime of p^+, noted $p^{+*}(\gamma)$. Oscillating regimes with higher periodicities which may appear between $\gamma = 1/3$ and $\gamma = 1/2$ are not represented.

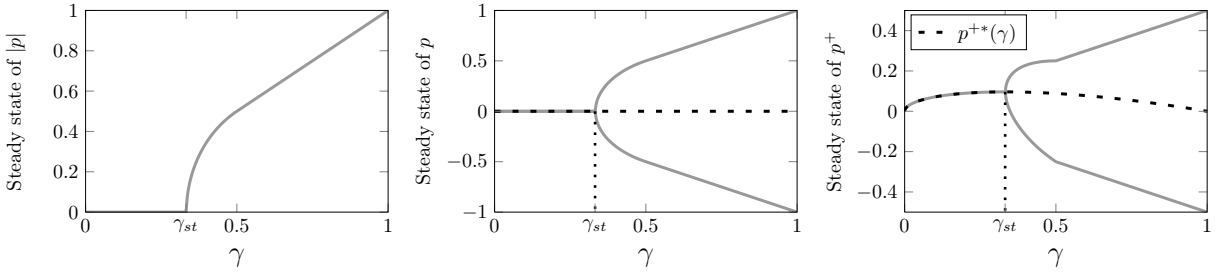

Figure 3: Graphical representation of the static bifurcation diagrams for $\zeta = 0.5$. From left to right: diagram based on variables $|p|$, p and p^+.

3 Time-varying blowing pressure

3.1 Problem statement

3.1.1 Definitions

Before presenting the problem, some definitions are introduced in order to avoid ambiguity in the vocabulary used hereafter. In the remainder of this paper, all simulations and calculations will be performed considering that the parameter ζ is a constant, although its value may vary from one simu-

lation to another. The definitions presented below, used commonly in works dealing with bifurcation theory, can present some conflicts with that of musical acoustics. The terms that will be used in the remaining discussions are clarified in the following paragraphs:

Static case The control parameter γ is constant and the system is described by:

$$p_n^+ = G_\gamma\left(p_{n-1}^+\right). \tag{22}$$

The steady state of the series p_n^+ depends on the value of the control parameter γ. If γ is smaller than γ_{st}, the series tends to a static regime. To avoid confusion, the static regime will now be called *non-oscillating static regime*. If γ is larger than γ_{st} the steady state of p_n^+ is an oscillating regime. This regime is called *oscillating static regime*. This behavior is still static, obtained by choosing a value of γ, letting the system reach its steady state, and repeating the procedure for each value of γ. Note that, even if the system tends to a steady state, the initial condition p_0^+ often induces a transient regime.

Dynamic case The control parameter γ is variable, now written as γ_n. When γ is a linear function of time, the system is described by the following difference equations:

$$\begin{cases} p_n^+ = G\left(p_{n-1}^+, \gamma_n\right) & \text{(23a)} \\ \gamma_n = \gamma_{n-1} + \epsilon. & \text{(23b)} \end{cases}$$

A slowly varying parameter implies that ϵ is arbitrarily small ($\epsilon \ll 1$). An example of a numerical simulation performed on the system (23) is shown in Fig. 4 for $\zeta = 0.5$, $\epsilon = 10^{-3}$ and an initial condition $\gamma_0 = 0.2$. The initial value of the outgoing wave is $p_0^+ = G(-p_0^- = 0, \gamma_0)$. Indeed, for $n = 0$ the incoming wave p^- is clearly zero, otherwise sound would have traveled back and forth with an infinite velocity.

The series p_n^+ first shows a short oscillating transient, which will be called *transient oscillating dynamic regime*. This oscillation decays into a *non-oscillating dynamic regime*. Beyond a certain threshold, a new oscillation grows, giving rise to the *final oscillating dynamic regime*.

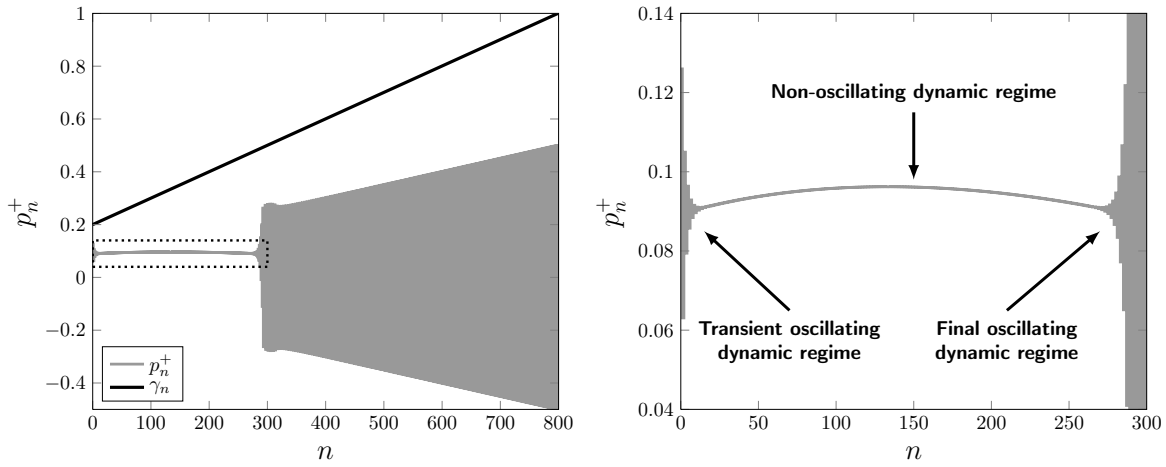

Figure 4: Numerical simulation performed on the system (23). (a) complete orbit of the series and (b) zoom near the non-oscillation dynamic regime. $\zeta = 0.5$, $\epsilon = 10^{-3}$, $\gamma_0 = 0.2$ and $p_0^+ = G(0, \gamma_0)$.

This paper will focus on the transition (i.e. the bifurcation) from the *non-oscillating dynamic regime* to the *final oscillating dynamic regime*. The value of the parameter γ for which the bifurcation occurs is called *dynamic oscillation threshold*, noted γ_{dt}.

3.1.2 Bifurcation delay

Bifurcation delay occurs in nonlinear-systems with time varying control parameters. Fruchard and Schäfke [11] published an overview of the problem of bifurcation delay.

In fig. 5, the system (23) was simulated numerically, showing the time evolution of the series p_n^+ and of the control parameter γ_n (cf. Fig. 5(a)). To better understand the consequence of a time-varying parameter, the orbit of the series p_n^+ is plotted as a function of the parameter γ_n – in this case the evolution of the system can be interpreted as a *dynamic bifurcation diagram*. This is compared to the static bifurcation diagram in Fig. 5(b). We can observe that the static and the dynamic oscillation diagrams coincide far from the static oscillation threshold γ_{st}. However, in the dynamic case, we can see that the orbit continues to follow closely the branch of the fixed point of function G throughout a remarkable extent of its unstable range, i.e. after γ_{st}: the bifurcation point is shifted from the static oscillation threshold γ_{st} to the dynamic oscillation threshold γ_{dt}. The term *bifurcation delay* is used to state the fact that the static oscillation threshold γ_{st} is smaller than the dynamic oscillation threshold γ_{dt}.

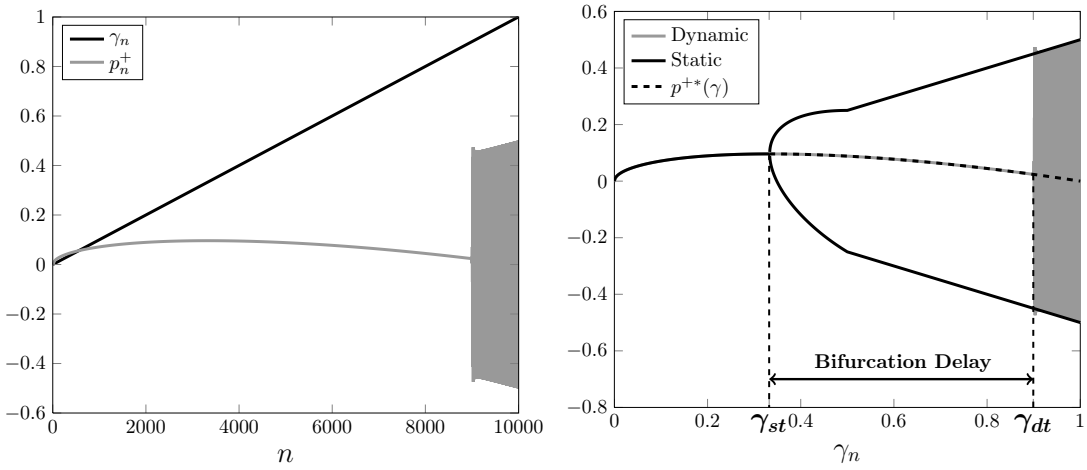

(a) (b)

Figure 5: (a) Time evolution of the series p_n^+ and of the control parameter γ_n.(b) Comparison between the series p_n^+ and the *static* bifurcation diagram as a function of γ_n. $\zeta = 0.5$, $\epsilon = 10^{-4}$, $\gamma_0 = 0$ and $p_0^+ = G(0, \gamma_0)$.

Non-standard analysis has been used in the past to study the phenomenon of bifurcation delay [16, 17], explaing that one of the causes of the bifurcation delay is the exponential proximity between the orbit of the series p_n^+ and the curve of the the fixed point of G. Other studies of bifurcation delay using standard mathematical tools – mathematics [10, 18] or physics publications [9, 19] – explain bifurcation delay as an accumulation of stability during the range of γ for which the fixed point of G is stable (i.e. $0 < \gamma_n < \gamma_{st}$). The dynamic oscillation threshold therefore appears as the value of the parameter γ at which the stability previously accumulated is compensated.

In musical acoustics literature some papers present results showing the phenomenon of bifurcation delay without never making a connection to the concept of *dynamic bifurcation*. For example this phenomenon is observed in simulations of clarinet-like systems using a slightly more sophisticated clarinet model (Raman's model) [20]. Raman's model takes losses into account although they are assumed to be independent of frequency (see [5] for further explanation). Bifurcation delay can also explain the difficulty in estimating the static oscillation threshold by using a slowly variable blowing pressure [21]. In a preliminary work [22], bifurcation delays were experimentally observed in a clarinet-like instrument.

3.2 Analytical study of the dynamic case

This section presents an analytical description of a clarinet-like system in a dynamic case. The notion of *invariant curve* ($\phi(\gamma, \epsilon)$), invariant under the mapping (23), will be needed for this study. The study of the stability of the invariant curve allows to define an analytical estimation of the dynamic

oscillation threshold. A generic method to calculate the invariant curve is given by Baesens [10][a], based on a perturbation method [23].

3.2.1 Invariant curve

The invariant curve $\phi(\gamma, \epsilon)$ is invariant under the mapping (23), satisfying the following equation:

$$\phi(\gamma, \epsilon) = G\left(\phi(\gamma - \epsilon, \epsilon), \gamma\right). \tag{24}$$

This curve plays a similar role for the dynamic system as fixed points for the static system, attracting or repelling the orbits. It is independent of the initial condition.

First of all, the invariant curve is expanded into a power series of ϵ, here truncated to the first order:

$$\phi(\gamma, \epsilon) \approx \phi_0(\gamma) + \epsilon\phi_1(\gamma). \tag{25}$$

Fig. 5 shows that, during the dynamic phase, the orbit of the series p_n^+ closely follows the curve of the fixed points of G. This allows to linearize function G around the curve of the fixed points $p^{+*}(\gamma)$:

$$G(x, \gamma) \approx G\left(p^{+*}(\gamma), \gamma\right) + \left[x - p^{+*}(\gamma)\right] \partial_x G\left(p^{+*}(\gamma), \gamma\right), \tag{26}$$

using the notation

$$\partial_x G\left(x, y\right) = \frac{\partial G(x, y)}{\partial x}, \tag{27}$$

and knowing that $G\left(p^{+*}(\gamma), \gamma\right) = p^{+*}(\gamma)$ (cf. equation (18)). Finally, using a Taylor expansion of $\phi(\gamma - \epsilon, \epsilon)$ equation (24) is successively solved for the functions $\phi_0(\gamma)$ and $\phi_1(\gamma)$, yielding:

$$\phi(\gamma, \epsilon) \approx p^{+*}(\gamma) \; + \; \epsilon \, \frac{dp^{+*}(\gamma)}{d\gamma} \, \frac{\partial_x G\left(p^{+*}(\gamma), \gamma\right)}{\partial_x G\left(p^{+*}(\gamma), \gamma\right) - 1}. \tag{28}$$

Using the explicit expressions of p^{+*} and $dp^{+*}/d\gamma$ we have:

$$\phi(\gamma, \epsilon) \approx \frac{\zeta}{2}\left[(1-\gamma)\sqrt{\gamma} \; - \; \epsilon \, \frac{(3\,\gamma - 1)}{2\,\sqrt{\gamma}} \, \frac{\partial_x G\left(p^{+*}(\gamma), \gamma\right)}{\partial_x G\left(p^{+*}(\gamma), \gamma\right) - 1}\right]. \tag{29}$$

More details about the calculation of the invariant curve are given in B.

To simplify the notation, in the rest of the document the invariant curve will be noted $\phi(\gamma)$. Its dependency on parameter ϵ is not explicitly stated.

[a] In [10] the invariant curve is called *adiabatic invariant manifold*.

3.2.2 Stability of the invariant curve and theoretical estimation of the dynamic oscillation threshold

A theoretical estimation of the dynamic oscillation threshold is done by identifying the value of γ for which the invariant curve looses its stability. The invariant curve is said to be unstable when the orbit of of the series p_n^+ escapes from the neighborhood of the invariant curve $\phi(\gamma, \epsilon)$.

To investigate the stability of the invariant curve $\phi(\gamma, \epsilon)$, the function G in equation (23a) is expanded in a first-order Taylor series around the invariant curve [10]:

$$\begin{aligned} p_n^+ &= G(p_{n-1}^+, \gamma_n) \\ &\approx G\left(\phi(\gamma_n - \epsilon), \gamma_n\right) + \left[p_{n-1}^+ - \phi(\gamma_n - \epsilon)\right] \partial_x G\left(\phi(\gamma_n - \epsilon), \gamma_n\right). \end{aligned} \tag{30}$$

A new variable is defined that describes the distance between the actual orbit and the invariant curve:

$$w_n = p_n^+ - \phi(\gamma_n), \tag{31}$$

and using equation (24), equation (30) becomes:

$$w_n = w_{n-1} \partial_x G\left(\phi(\gamma_n - \epsilon), \gamma_n\right). \tag{32}$$

The solution of equation (32) is formally:

$$w_n = w_0 \prod_{i=1}^{n} \partial_x G\left(\phi(\gamma_i - \epsilon), \gamma_i\right), \tag{33}$$

for $n \geq 1$ and where w_0 is the initial value of w_n. The absolute value of w_n can be written as follow:

$$|w_n| = |w_0| \exp\left(\sum_{i=1}^{n} \ln\left|\partial_x G\left(\phi(\gamma_i - \epsilon), \gamma_i\right)\right|\right). \tag{34}$$

Finally, using Euler's approximation the sum is replaced by an integral:

$$|w_n| \approx |w_0| \exp\left(\int_{\gamma_0+\epsilon}^{\gamma_n+\epsilon} \ln\left|\partial_x G\left(\phi(\gamma' - \epsilon), \gamma'\right)\right| \frac{d\gamma'}{\epsilon}\right). \tag{35}$$

Equation (35) shows that the variable p^+ starts to diverge from the invariant curve $\phi(\gamma, \epsilon)$ when the argument of the exponential function changes from negative to positive. Therefore, the analytical estimation of the dynamic oscillation threshold γ_{dt}^{th} is defined by:

$$\int_{\gamma_0+\epsilon}^{\gamma_{dt}^{th}+\epsilon} \ln\left|\partial_x G\left(\phi(\gamma'-\epsilon),\gamma'\right)\right| d\gamma' = 0, \tag{36}$$

where γ_0 is the initial value of γ. This result can be deduced from [10] (equation (2.18)), it may also be obtained in the framework of non-standard analysis [24].

The theoretical estimation γ_{dt}^{th} of the dynamic oscillation threshold depends on the initial condition γ_0 and on the increase rate ϵ, it is therefore written $\gamma_{dt}^{th}(\gamma_0,\epsilon)$.

A numerical solution $\gamma_{dt}^{th}(\gamma_0,\epsilon)$ of the implicit equation (36) is plotted in Fig. 6 as a function of the initial condition γ_0 and for $\epsilon = 10^{-2}$, 10^{-3} and 10^{-4}. γ_{dt}^{th} can be much larger than static oscillation threshold $\gamma_{st} = 1/3$ for small initial conditions γ_0. When the initial condition value γ_0 increases, γ_{dt}^{th} approaches the static threshold. Fig. 6(d) shows that the bifurcation delay seems to be independent of the increase rate ϵ if this value is sufficiently small (typically $\leq 10^{-3}$).

Equation (36) states that when $\gamma = \gamma_{dt}^{th}$ we have $|w_n| \approx |w_0|$, providing a good estimation of the dynamic oscillation threshold γ_{dt} if $|w_0|$ is sufficiently small, i.e. if p_0^+ is sufficiently close to $\phi(\gamma_0)$. $\gamma_0 = 0$ can be problematic since $\phi(0,\epsilon) = -\infty$, but a single iteration is sufficient to bring the orbit to a neighborhood of the invariant curve. Therefore, we make the assumption that

$$\gamma_{dt}^{th}(0,\epsilon) \approx \gamma_{dt}^{th}(\epsilon,\epsilon). \tag{37}$$

A non-exhaustive study done by running a few simulations shows that for $\epsilon = 10^{-4}$ the error in γ_{dt} due to this approximation is under 10^{-8}, rising to 10^{-7} when $\epsilon = 10^{-3}$ and 2×10^{-5} when $\epsilon = 10^{-2}$.

3.3 Benchmark of theoretical estimators for the dynamic threshold

Multiple criteria can be associated to the beginning of the oscillating regime. For instance, the oscillations can start before the series departs from the vicinity of the invariant curve as described in equation (36). Moreover, because of the approximation used between equations (35) and (36), the value of $\gamma = \gamma_{dt}^{th}$ may not be an accurate estimation of the value at which the orbit departs from this vicinity.

For comparison, a dynamic oscillation threshold (noted γ_{dt}^{num}) is calculated by simulating system (23) and compared with γ_{dt}^{th}. When the orbit of the series p_n^+ is periodic, the sign of the second order difference of p_n^+ changes sign at each iteration (i.e. the curve of p_n^+ changes from upward to downward concave). In discrete time formulation the second order difference is given by:

$$\left(d^2p^+\right)_i = \left(p_i^+ - p_{i-1}^+\right) - \left(p_{i-1}^+ - p_{i-2}^+\right). \tag{38}$$

Therefore, γ_{dt}^{num}, the oscillation threshold measured in numerical simulations, is reached when

$$\left(d^2p^+\right)_{i-1}\left(d^2p^+\right)_i < 0, \tag{39}$$

is satisfied.

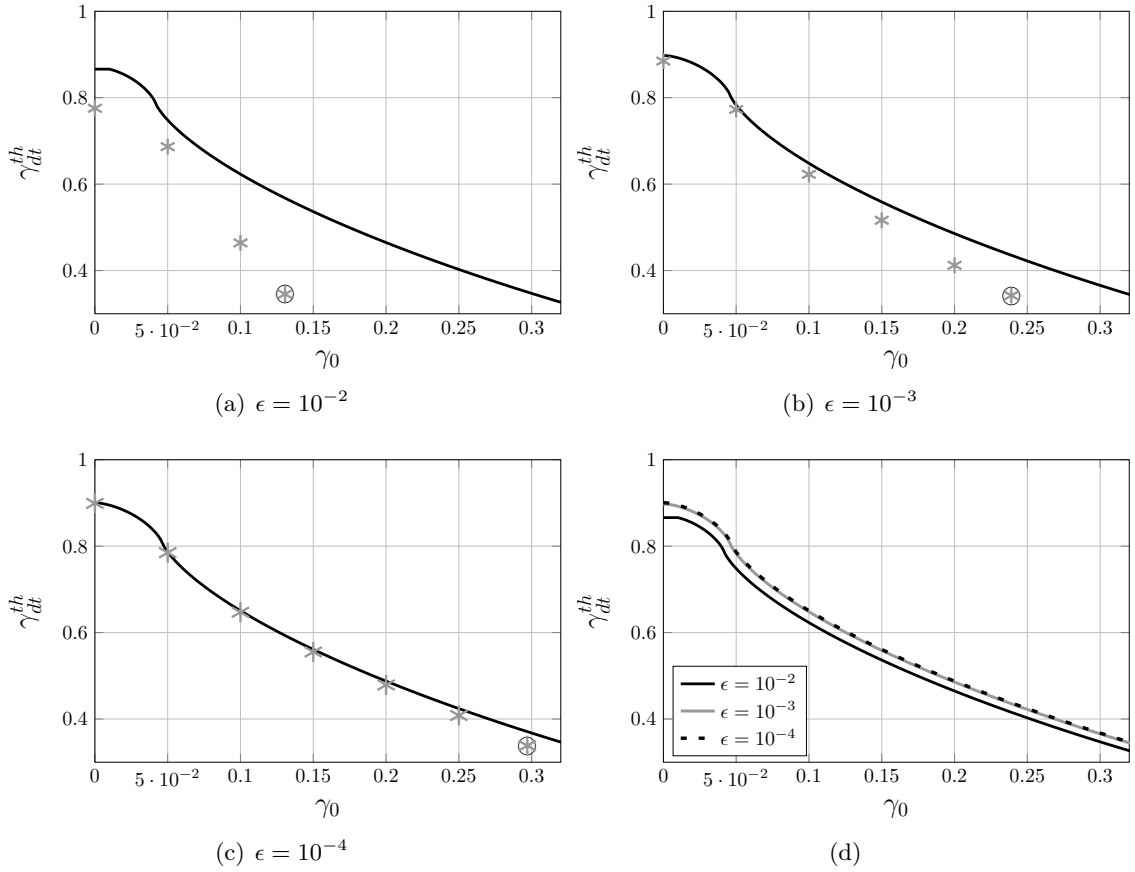

(a) $\epsilon = 10^{-2}$ (b) $\epsilon = 10^{-3}$

(c) $\epsilon = 10^{-4}$ (d)

Figure 6: Plot of γ_{dt} as a function of the initial condition γ_0, for different values of the slope ϵ. (a), (b) and (c): solid lines are the theoretical prediction γ_{dt}^{th} calculated from equation (36). Gray "$*$" markers represent the value γ_{dt}^{num} for which the system begins to oscillate. (d): combination of the previous theoretical predictions. "$\circledast$" represent the highest γ_0 for which the system has enough time to reach a non-oscillating dynamic regime.

Then, in Fig. 6, γ_{dt}^{num} is compared with γ_{dt}^{th} (gray "$*$" markers). In some cases the series p_n^+ never reaches the non-oscillating dynamic regime. An example of such situations is shown in Fig. 7. The values of γ_{dt}^{num} corresponding to the last initial values γ_0 for which the system has enough time to reach the non-oscillating dynamic regime are circled.

Fig. 6 shows that for $\epsilon = 10^{-4}$ the theoretical result γ_{dt}^{th} provides a good estimation of the observed dynamic oscillation threshold. For $\epsilon = 10^{-3}$, the theoretical estimation is also good if the the initial condition is sufficiently small but as γ_0 gets closer to the static threshold γ_{st} the system begins to oscillate before $\gamma = \gamma_{dt}^{th}$. Finally, for $\epsilon = 10^{-2}$, γ_{dt}^{num} is always smaller than γ_{dt}^{th}.

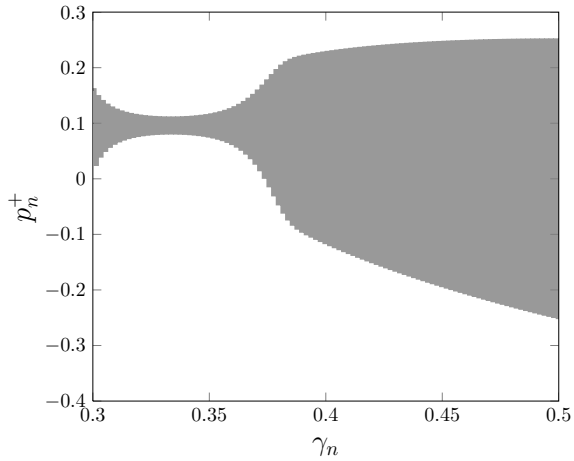

Figure 7: Representation of the series p_n^+ as a function of γ_n for $\zeta = 0.5$,$\epsilon = 10^{-3}$, $\gamma_0 = 0.3$ and $p_0^+ = G(0, \gamma_0)$.

4 Limit of the model: influence of the precision

The phenomenon of bifurcation delay is very sensitive to noise: either numerical noise (round-off errors of the computer) or experimental noise (due to turbulence for instance). Indeed, when the static threshold is exceeded the system is very unstable. As a result, to observe bifurcation delay with numerical simulations and compare to theoretical results, it is necessary to perform calculations using a very high precision, as was done previously in this paper. For lower precisions the bifurcation delay can be considerably reduced (see [17] for an example in the logistic map).

Fig. 8 shows an example of numerical simulation performed on system (23). Fig. 8(a) and Fig. 8(b) differ only in the numerical precision (i.e. the number of decimal digits) used to calculate the orbit. The choice of the precision is possible using *mpmath*, the arbitrary precision library of *Python*. Fig. 8(a) was obtained using a precision of 5000 decimal digits, in this case γ_{dt}^{th} gives a good estimation of the bifurcation point, as it has already been shown in Fig. 6. On the other hand, using a precision of 15 decimal digits (Fig. 8(b)), the bifurcation delay is considerably reduced and the theoretical estimation of the dynamic oscillation threshold is not valid.

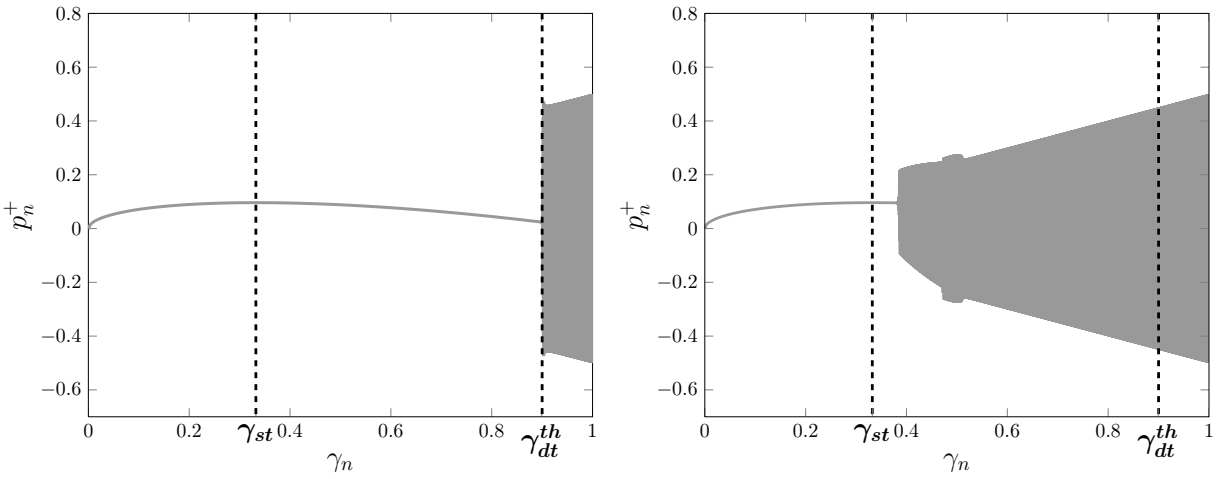

(a) precision = 5000

(b) precision = 15

Figure 8: Representation of the series p_n^+ for $\zeta = 0.5$, $\epsilon = 10^{-4}$, $\gamma_0 = 0$, $p_0^+ = G(0, \gamma_0)$ and for two different values of the precision.

To highlight the influence of the precision γ_{dt}^{num} is calculated for different precisions. Results are plotted in Fig. 9 and compared to the analytical values γ_{st} and γ_{dt}^{th}.

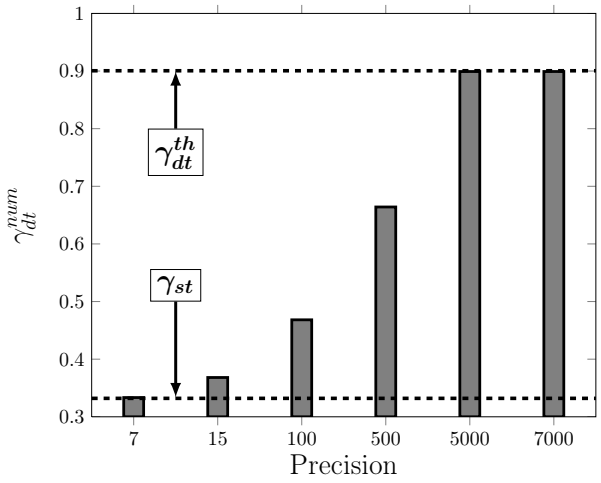

Figure 9: Graphical representation of γ_{dt}^{num} for different precisions (prec. = 7, 15, 100, 500 and 5000) and for $\epsilon = 10^{-4}$. Results are also compared to analytical *static* and *dynamic* thresholds: γ_{st} and γ_{dt}^{th}. $\zeta = 0.5$ and $\gamma_0 = 0$.

The first thing to observe in Fig. 9 is the very high sensitivity of γ_{dt}^{num} to precision, yet all the values of γ_{dt}^{num} appear between γ_{st} and γ_{dt}^{th}. For the lowest precision (7 decimal digits) the bifurcation delay disappears and $\gamma_{dt}^{num} = \gamma_{st}$. If the precision is very high (5000 decimals) $\gamma_{dt}^{num} = \gamma_{dt}^{th}$. Therefore, γ_{dt}^{th} can be interpreted as the limit of the bifurcation delay when precision tends to infinity. In cases with intermediate precisions (prec. = 15, 100 and 500) the bifurcation delay increases with the precision.

The sensitivity to the precision depends on the value of the increase rate ϵ: Fig. 10 plots γ_{dt}^{num} with

respect to ϵ for different values of the numerical precision. Results are also compared with γ_{st} and γ_{dt}^{th}.

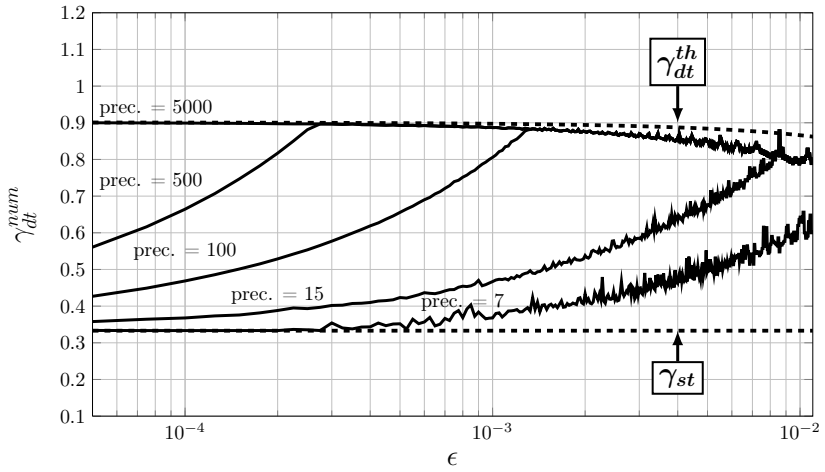

Figure 10: Graphical representation of γ_{dt}^{num} as a function of ϵ for $\zeta = 0.5$ and using five different precisions. A logarithmic scale is used in abscissa.

As above, for the lowest precision (7 decimals) the bifurcation delay disappears when ϵ is sufficiently small. Indeed, γ_{dt}^{num} is constant and equal to γ_{st}. Then bifurcation delay occurs and increases with ϵ. The case of the highest precision (5000 decimals) is identical to an analytical case which would correspond to infinite precision. When ϵ is sufficiently small, the curves of γ_{dt}^{num} and γ_{dt}^{th} overlap. In this case when ϵ is small γ_{dt}^{num} is almost constant suggesting that the bifurcation delay does not depend on the increase rate, as previously shown in Fig. 6(d). Then, still in the case of a precision of 5000 decimals, γ_{dt}^{num} decreases for increasing ϵ, and γ_{dt}^{th} also decreases but to a lesser extent. For intermediate precisions (15, 100 and 500 decimals) the curve of γ_{dt}^{num} first increases before stabilizing close to the curve of γ_{dt}^{th}. For a given value of the precision, the larger the ϵ, the smaller is the accumulation of round-off errors created by the computer to reach a certain value of γ. This explains why the bifurcation delay first increases if the precision is not sufficiently high to simulate an analytic case. Beyond a certain value, all curves coincide with the one corresponding to the highest precision. That means that the system has reached the pair of parameters [precison ; ϵ] needed to simulate an analytic case.

5 Conclusion

When considering mathematical models of musical instruments, oscillation threshold obtained through a static bifurcation analysis may be possibly very different from the threshold detected on a numerical simulation of this model.

For the first time for musical instruments, the differences between these two thresholds have been interpreted as the appearance of the phenomenon of *bifurcation delay* in connection with the concept

of *dynamic bifurcation*.

Theoretical estimations of the dynamic bifurcation provided in this paper have to be compared with care to numerical simulations since the numerical precision used in computations plays a key role: for numerical precisions close to standard machine precision, the bifurcation towards the oscillating regime can occur at significantly lower mouth pressure values (while different most of the time from the threshold obtained through static bifurcation theory). Moreover, in that case, the threshold at which the oscillations start becomes more dependent on the increase rate of the mouth pressure.

The dependency on precision can be linked to the influence of noise generated by turbulence as the musician blows into the instrument. This would explain why the delays observed in artificially blown instruments are shorter than the predicted theoretical ones. This will be the subject of further work on this subject, as well as the validity of these results for smoother curves of variation of the mouth pressure.

Moreover, in the light of results presented here for a basic model of wind instruments, varying the blowing pressure (even slowly) does not appear as the best way to experimentally determine Hopf bifurcations (static). In a musical context, since the blowing pressure varies through time, the dynamic threshold is likely to give more relevant informations than the static threshold, even if, in a real situation the influence of noise must be considered.

As a final remark, the simplistic model used in this work only describes one point per half-period of the sound played by the instrument. It is thus not suitable to describe different regimes (whose frequencies are harmonics of the fundamental one) that can be obtained by the instrument. However a simple extension of this model calculating the orbits of different instants within the half-period may be able to provide some insight on this subject.

Acknowledgments

We wish to thank Mr Jean Kergomard for his valuable comments on the manuscript.

This work was done within the framework of the project SDNS-AIMV "Systèmes Dynamiques Non-Stationnaires - Application aux Instruments à Vent" financed by *Agence Nationale de la Recherche* (ANR).

A Table of notation

Physical variables		
Symbol	**Explanation**	**Unit**
Z_c	characteristic impedance	$\mathrm{Pa{\cdot}s{\cdot}m^{-1}}$
K_s	static stiffness of the reed	$\mathrm{Pa{\cdot}m^{-1}}$
P_M	static closing pressure of the reed	Pa
H	opening height of the reed channel at rest	m
U	flow created by the pressure imbalance between the mouth and the mouthpiece	$\mathrm{m^3{\cdot}s^{-1}}$
U_r	flow created by the motion of the reed	$\mathrm{m^3{\cdot}s^{-1}}$
U_{in}	flow at the entrance of the resonator	$\mathrm{m^3{\cdot}s^{-1}}$
U_A	flow amplitude parameter	$\mathrm{m^3{\cdot}s^{-1}}$
P_m	musician mouth pressure	Pa
P	pressure inside the mouthpiece	Pa
ΔP	pressure difference $P_m - P$	Pa
y	displacement of the tip of the reed	m
τ	round trip travel time of a wave along the resonator	m

Dimensionless variables	
Symbol	**Associated physical variable**
γ	musician mouth pressure
ζ	flow amplitude parameter
u	flow at the entrance of the resonator
p	pressure inside the mouthpiece
r	reflexion function of the resonator
p^+	outgoing wave
p^-	incoming wave
p^{+*}	non-oscillating static regime of p^+ (fixed points of the function G)
ϕ	invariant curve
w	difference between p^+ and ϕ
ϵ	increase rate of the parameter γ
γ_{st}	static oscillation threshold
γ_{dt}	dynamic oscillation threshold
γ_{dt}^{th}	theoretical estimation of the dynamic oscillation threshold
γ_{dt}^{num}	value of γ when the system begins to oscillate (calculated numerically)

Nonlinear characteristic of the embouchure		
Function	**Associated representation**	**Definition**
F	$\{u\,;\,p\}$	$u = F(p)$
G	$\{p^+\,;\,p^-\}$	$p^+ = G(-p^-)$

B Invariant curve

The invariant curve $\phi(\gamma, \epsilon)$ is invariant under the mapping (23), it therefore satisfies the following equation:

$$\phi(\gamma, \epsilon) = G\left(\phi(\gamma - \epsilon, \epsilon), \gamma\right). \tag{40}$$

First of all, the invariant curve is expanded into a power series of ϵ and only he first-order is retained:

$$\phi(\gamma,\epsilon) \approx \phi_0(\gamma) + \epsilon\phi_1(\gamma). \tag{41}$$

Secondly, the function G is linearized around the curve $p^{+*}(\gamma)$ of the fixed points:

$$\begin{aligned} G(x,\gamma) &\approx G\left(p^{+*}(\gamma),\gamma\right) + \left[x - p^{+*}(\gamma)\right]\partial_x G\left(p^{+*}(\gamma),\gamma\right) &(42)\\ &= p^{+*}(\gamma) + \left[x - p^{+*}(\gamma)\right]\partial_x G\left(p^{+*}(\gamma),\gamma\right) &(43)\end{aligned}$$

where

$$\partial_x G\left(x,y\right) = \frac{\partial G(x,y)}{\partial x}. \tag{44}$$

Then, we make a Taylor expansion of $\phi(\gamma-\epsilon,\epsilon)$:

$$\begin{aligned} \phi(\gamma-\epsilon,\epsilon) &\approx \phi(\gamma,\epsilon) - \epsilon\frac{\partial u}{\partial\gamma}(\gamma,\epsilon) + O(\epsilon^2); &(45)\\ &= \phi_0(\gamma) + \epsilon\phi_1(\gamma) - \epsilon\frac{\partial u_0(\gamma)}{\partial\gamma} + O(\epsilon^2). &(46)\end{aligned}$$

Finally, neglecting the second-order terms in ϵ, equation (40) becomes:

$$\phi_0(\gamma) + \epsilon\phi_1(\gamma) = p^{+*}(\gamma) + \left[\phi_0(\gamma) + \epsilon\phi_1(\gamma) - \epsilon\frac{\partial\phi_0(\gamma)}{\partial\gamma} - p^{+*}(\gamma)\right]\partial_x G\left(p^{+*}(\gamma),\gamma\right). \tag{47}$$

To obtain the approximate analytical expression of the invariant cure ϕ, equation (47) is successively solved for the functions $\phi_0(\gamma)$ and $\phi_1(\gamma)$.

To order 0, we have to solve:

$$\phi_0(\gamma) = p^{+*}(\gamma) + \left[\phi_0(\gamma) - p^{+*}(\gamma)\right]\partial_x G\left(p^{+*}(\gamma),\gamma\right). \tag{48}$$

Therefore the expression of $\phi_0(\gamma)$ is:

$$\begin{aligned} \phi_0(\gamma) &= p^{+*}(\gamma)\frac{1-\partial_x G\left(p^{+*}(\gamma),\gamma\right)}{1-\partial_x G\left(p^{+*}(\gamma),\gamma\right)}; &(49)\\ &= p^{+*}(\gamma). &(50)\end{aligned}$$

To order 1, we have to solve:

$$\phi_1(\gamma) = \left[\phi_1(\gamma) - \frac{\partial \phi_0(\gamma)}{\partial \gamma}\right] \partial_x G\left(p^{+*}(\gamma), \gamma\right); \quad (51)$$

$$= \left[\phi_1(\gamma) - \frac{\partial p^{+*}(\gamma)}{\partial \gamma}\right] \partial_x G\left(p^{+*}(\gamma), \gamma\right), \quad (52)$$

and therefore:

$$\phi_1(\gamma) = \frac{\partial p^{+*}(\gamma)}{\partial \gamma} \frac{\partial_x G\left(p^{+*}(\gamma), \gamma\right)}{\partial_x G\left(p^{+*}(\gamma), \gamma\right) - 1} \quad (53)$$

Finally the expression of the invariant curve is:

$$\phi(\gamma, \epsilon) \approx p^{+*}(\gamma) \; + \; \epsilon \, \frac{\partial p^{+*}(\gamma)}{\partial \gamma} \; \frac{\partial_x G\left(p^{+*}(\gamma), \gamma\right)}{\partial_x G\left(p^{+*}(\gamma), \gamma\right) - 1}. \quad (54)$$

References

References

[1] M. E. Mcintyre, R. T. Schumacher, and J. Woodhouse. On the oscillations of musical instruments. *J. Acoust. Soc. Am.*, 74(5):1325–1345, November 1983.

[2] C. Maganza, R. Caussé, and F. Laloë. Bifurcations, period doublings and chaos in clarinet-like systems. *EPL (Europhysics Letters)*, 1(6):295, 1986.

[3] J. Kergomard. Elementary considerations on reed-instrument oscillations. In *Mechanics of musical instruments by A. Hirschberg/ J. Kergomard/ G. Weinreich*, volume 335 of *CISM Courses and lectures*, chapter 6, pages 229–290. Springer-Verlag, 1995.

[4] A. Chaigne and J. Kergomard. Instruments à anche. In *Acoustique des instruments de musique*, chapter 9, pages 400–468. Belin, 2008.

[5] J.P. Dalmont, J. Gilbert, J. Kergomard, and S. Ollivier. An analytical prediction of the oscillation and extinction thresholds of a clarinet. *J. Acoust. Soc. Am.*, 118(5):3294–3305, 2005.

[6] S. Ollivier, J. P. Dalmont, and J. Kergomard. Idealized models of reed woodwinds. part 2 : On the stability of two-step oscillations. *Acta. Acust. united Ac.*, 91:166–179, 2005.

[7] J. Kergomard, J. P. Dalmont, J. Gilbert, and P. Guillemain. Period doubling on cylindrical reed instruments. In *Proceeding of the Joint congress CFA/DAGA 04*, pages 113–114. Société Française d'Acoustique - Deutsche Gesellschaft für Akustik, 22nd-24th March 2004, Strasbourg, France.

[8] P.A. Taillard, J. Kergomard, and F. Laloë. Iterated maps for clarinet-like systems. *Nonlinear Dyn.*, 62:253–271, 2010.

[9] R. Kapral and P. Mandel. Bifurcation structure of the nonautonomous quadratic map. *Phys. Rev. A*, 32(2):1076–1081, 1985.

[10] C. Baesens. Slow sweep through a period-doubling cascade: Delayed bifurcations and renormalisation. *Physica D*, 53:319–375, 1991.

[11] A. Fruchard and R. Schäfke. Sur le retard à la bifurcation. In *International conference in honor of claude Lobry*, 2007.

[12] A. Hirschberg, R. W. A. Van de Laar, J. P. Maurires, A. P. J Wijnands, H. J. Dane, S. G. Kruijswijk, and A. J. M. Houtsma. A quasi-stationary model of air flow in the reed channel of single-reed woodwind instruments. *Acustica*, 70:146–154, 1990.

[13] A. Hirschberg. Aero-acoustics of wind instruments. In *Mechanics of musical instruments by A. Hirschberg/ J. Kergomard/ G. Weinreich*, volume 335 of *CISM Courses and lectures*, chapter 7, pages 291–361. Springer-Verlag, 1995.

[14] J. Kergomard. *Mechanics of musical instruments.* chap. 6, p. 229-290. N° 355 in CISM courses and lectures, Springer-Verlag, New York, 1995.

[15] M. J. Feigenbaum. The universal metric properties of nonlinear transformations. *J. Stat. Phy.*, 21(6):669–706, 1979.

[16] A. Fruchard. Sur l'équation aux différences affine du premier ordre unidimensionnelle. *Ann. Inst. Fourier*, 46(1):139–181, 1996.

[17] A. Fruchard and R. Schäfke. Bifurcation delay and difference equations. *Nonlinearity*, 16:2199–2220, 2003.

[18] C. Baesens. Gevrey series and dynamic bifurcations for analytic slow-fast mappings. *Nonlinearity*, 8:179–201, 1995.

[19] J. R. Tredicce, G.L. Lippi, P. Mandel, B. Charasse, A. Chevalier, and B. Picqué. Critical slowing down at a bifurcation. *Am. J. Phys.*, 72(6):799–809, 2004.

[20] M. Atig, J. P. Dalmont, and J. Gilbert. Saturation mechanism in clarinet-like instruments, the effect of the localised nonlinear losses. *Appl. Acoust.*, 65(12):1133–1154, 2004.

[21] D. Ferrand, C. Vergez, and F. Silva. Seuils d'oscillation de la clarinette : validité de la représentation excitateur-résonateur. In *10ème Congrès Français d'Acoustique*, Lyon, France, April 12nd-16th 2010.

[22] B. Bergeot, C. Vergez, A. Almeida, and B. Gazengel. Measurement of attack transients in a clarinet driven by a ramp-like varying pressure. In *11ème Congrès Français d'Acoustique and 2012 Annual IOA Meeting*, Nantes, France, April 23rd-27th 2012.

[23] C.M. Bender and S.A. Orszag. *Advanced mathematical methods for scientists and engineers.* McGraw-Hill Book Company, 1987.

[24] A. Fruchard. Canards et râteaux. *Ann. Inst. Fourier*, 42(4):825–855, 1992.